energies

MDPI

Article

The Equivalent Effect of Initial Condition Coupling on the Laminar Burning Velocity of Natural Gas Diluted by CO_2

Xueshun Wu [1], Peng Wang [1], Zhennan Zhu [2], Yunshou Qian [1], Wenbin Yu [3,*] and Zhiqiang Han [4]

[1] Key Laboratory of Fluid and Power Machinery, Ministry of Education, Xihua University, Chengdu 610039, China; xueshunwu08@mail.xhu.edu.cn (X.W.); josen.wpeng@foxmail.com (P.W.); qianyuns@sinocat.com.cn (Y.Q.)
[2] Department of Engineering and Design, University of Sussex, Brighton BN1 9QT, UK; zz293@sussex.ac.uk
[3] School of Energy and Power Engineering, Shandong University, Jinan 117576, China
[4] Key Laboratory of Automobile Measurement Control and Safety in Sichuan Province, Xihua University, Chengdu 610039, China; hanzq@mail.xhu.edu.cn
* Correspondence: wbyu@u.nus.edu

Abstract: Initial temperature has a promoting effect on laminar burning velocity, while initial pressure and dilution rate have an inhibitory effect on laminar burning velocity. Equal laminar burning velocities can be obtained by initial condition coupling with different temperatures, pressures and dilution rates. This paper analysed the equivalent distribution pattern of laminar burning velocity and the variation pattern of an equal weight curve using the coupling effect of the initial pressure (0.1–0.3 MPa), initial temperature (323–423 K) and dilution rate (0–16%). The results show that, as the initial temperature increases, the initial pressure decreases and the dilution rate decreases, the rate of change in laminar burning velocity increases. The equivalent effect of initial condition coupling can obtain equal laminar burning velocity with an dilution rate increase (or decrease) of 2% and an initial temperature increase (or decrease) of 29 K. Moreover, the increase in equivalence ratio leads to the rate of change in laminar burning velocity first increasing and then decreasing, while the increases in dilution rate and initial pressure make the rate of change in laminar burning velocity gradually decrease and the increase in initial temperature makes the rate of change in laminar burning velocity gradually increase. The area of the region, where the initial temperature influence weight is larger, gradually decreases as the dilution rate increases, and the rate of decrease gradually decreases.

Keywords: natural gas; laminar burning velocity; equivalent effect; influence weight

Citation: Wu, X.; Wang, P.; Zhu, Z.; Qian, Y.; Yu, W.; Han, Z. The Equivalent Effect of Initial Condition Coupling on the Laminar Burning Velocity of Natural Gas Diluted by CO_2. *Energies* **2021**, *14*, 809. https://doi.org/10.3390/en14040809

Received: 29 December 2020
Accepted: 31 January 2021
Published: 4 February 2021

1. Introduction

Natural gas is considered the oil alternative fuel with the most potential due to its advantages of eco-friendliness, cleanliness, low carbon emission, high efficiency and low price, which have attracted the attention of scholars at home and abroad [1–3]. The laminar burning characteristics of natural gas are of great significance for understanding the inherent physical and chemical properties, the flame propagation process and the chemical kinetics [4–6]. Domestic and international scholars have conducted a lot of research regarding the influence of initial pressure (Pu), initial temperature (Tu), mixed gas composition and concentration on laminar burning velocity (u_L). Han et al. [7] analysed the effect of initial temperature (323–423 K) on the laminar flame of premixed natural gas through experimental studies. The results show that, with the increase in Tu, u_L gradually increases. Hermanns et al. [8] summarised the available measurements of laminar burning velocities in $CH_4 + H_2 + O_2 + N_2$ flames at a temperature range of 298–418 K performed using a heating flux method. The results show that the increase in Tu increases u_L under different equivalence ratios. Halter et al. [9] analysed the effect of Pu (0.1–0.5 MPa) on the laminar flame of CH_4/air mixtures through experimental studies. The results show that, with the increase in Pu, u_L gradually decreases. Xie et al. [10] carried

out a chemical kinetic modelling study of laminar burning characteristics for CH_4/CO_2 mixtures at elevated pressure by CHEMKIN coupling with a detailed chemical reaction mechanism. The results show that u_L decreases with increasing pressure under high pressure. Chan et al. [11] studied the effects of CO_2 diluent on u_L of CH_4/air premixed flames utilizing experimentation and kinetic modelling. The results show that u_L of the methane and air mixture decreases as the CO_2 dilution rate (DR) increases. Zhou et al. [12] conducted a study on the effect of diluents (N_2/CO_2) on the laminar flame speed of a $H_2/CO/CH_4$/air premixed flame using an outwardly propagating spherical flame and the CHEMKIN package. The results show that laminar flame speed decreases with the increase in N_2/CO_2 dilution ratios and that CO_2 dilution has a stronger dilution effect, thermal effect and chemical effect than those of N_2 dilution. Huang et al. [13] studied the laminar flame characteristics of natural gas–air flames in a constant-volume bomb at normal temperature and pressure. The results show that u_L tends to increase first and then decrease with the increase in the equivalence ratio (Φ), and the maximum value is obtained between Φ from 1.0 to 1.1. Dirrenberger et al. [14] presented new experimental measurements of the laminar flame velocity of natural gas with equivalence ratios from 0.6 to 2.1 performed by the heat flux method. The results show that, with the increase in Φ, u_L increases first and then decreases. This pattern maintains good consistency with other test data from the literature.

According to the above review, Tu has a promoting effect on u_L while Pu and DR have an inhibitory effect on u_L. Equal laminar burning velocities can be obtained by initial condition coupling with different temperatures, pressures and DRs. However, the literature lacks corresponding research results on the equivalent effect on laminar burning. There are much domestic and foreign research on the influence of parameters such as Tu, Pu and DR on combustion, but most of the research focuses on the influence of a single parameter on laminar burning, and it is difficult to obtain a quantitative equivalent relationship. Based on the equivalent laminar burning concept, this paper analysed the equivalent distribution pattern of u_L and the variation pattern of the equal weight curve by the coupling effects of Pu (0.1–0.3 MPa), Tu (323–423 K) and DR (0–16%). Relevant data support and engineering reference are provided for revealing the influence of the coupling mechanism of initial parameters on the laminar burning process, which is of great significance.

2. Experimental Setup

Figure 1 is a schematic of the test system, which is mainly composed of a constant volume chamber (CVC), a temperature monitoring system, an ignition system, a data acquisition system and a Schlieren imaging system [15]. The temperature monitoring system includes a K-Type thermocouple and a proportional-integral-derivative (PID) temperature controller, which is capable of maintaining the Tu error within ± 3 k. The parameters of the ignition system are as follows: the ignition voltage is 14 V, provided by a stabilized power supply; the ignition pulse width is 3 ms; the ignition electrode diameter is 2 mm; and the gap between the ignition electrodes is 3 mm. The data acquisition system includes a pressure sensor (KISTLER 6125C), a data acquisition card (Data acquisition, NiUSB-6365, sampling frequency of 100,000 Hz) and a charge amplifier (KISTLER 5018A). The Schlieren imaging system includes an illuminator (100 W Power), two concave mirrors (Focal length 110 mm), two plane mirrors and a high-speed digital camera (Phantom V7.3, 10,000 fps, resolution 512 $\times$ 512 pixels). Table 1 shows the main parameters of the CVC.

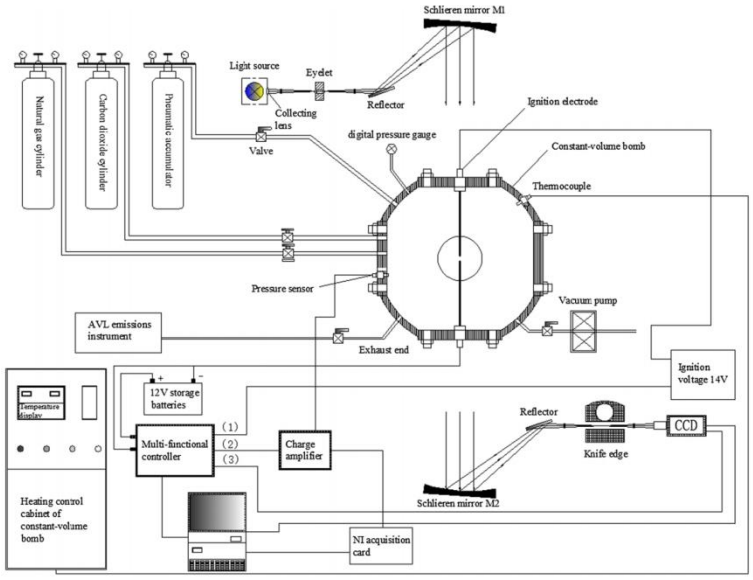

Figure 1. The experimental setup.

Table 1. Basic parameters of the constant volume chamber (CVC).

Parameter (Unit)	Value
Inner diameter (mm)	350
Volume (L)	22.4
Maximum heating temperature (K)	600
Maximum pressure (MPa)	4
Effective diameter of windows (mm)	Φ120

The experiment uses a mixture of CO_2, natural gas and compressed air to carry out premixed combustion research in order to meet the needs of modern society for natural gas engine performance simulation. CO_2 is used as an inert gas to reduce the oxygen concentration of the reactant, mainly to simulate the exhaust gas recirculation (EGR) technology of the engine. Compared with N_2, CO_2 has a greater impact on the laminar combustion of mixed gas, which is closer to the actual use of real EGR technology. In the test, gaseous CO_2, natural gas and compressed air are charged to the CVC to the specified pressure sequentially according to the law of partial pressure. The chemical reaction formula of the reaction between natural gas (CH_4) and oxygen (O_2) is as follows:

$$CH_4 + 2O_2 = CO_2 + 2H_2O \quad (1)$$

From the metering ratio of this reaction formula, it can be seen that 1 mol methane needs to consume 2 mol oxygen gas and that the source of oxygen is air. After calculation, at Φ of 1, the complete oxidation of 1 mol of methane needs to consume 9.524 mol of air.

The partial pressure of carbon dioxide is expressed as follows:

$$P_{CO_2} = DR \times Pu \quad (2)$$

When the equivalence ratio is Φ, the oxidation of 1 mol methane needs to consume 9.524/Φ mol air, so the partial pressure of methane when the equivalence ratio is Φ is as follows:

$$p_{CH_4} = \frac{Pu - P_{CO_2}}{1 + 9.524/\varphi} \quad (3)$$

The compressed air partial pressure is obtained from the total initial pressure minus other gas partial pressures:

$$P_{air} = Pu - P_{CO_2} - P_{CH_4} \quad (4)$$

The above method is used to complete the gas distribution of the constant volume chamber (CVC). Meanwhile, the gas is gradually heated to Tu. Let it stand for at least 5 min to achieve gas premixing. After the combustion is completed, the residual exhaust gas is discharged for "scrubbing" and vacuumed more than three times to ensure chamber cleanliness [16]. To reduce the test error [17–19], the radius of this test is 6–25 mm.

3. Data Processing

3.1. Extraction of Flame Radius

Figure 2 illustrates the process of obtaining a Schlieren image of the propagation flame radius using the commercial mathematical software MATLAB. This paper chose the Canny operator because of its high precision [20]. Before detecting the image boundary, five steps were applied: background removal, greyscale processing (the threshold value is 10), flame front extraction, boundary identification and fitting [21]. In the radius calculation, the horizontal line was rotated clockwise by 0 degrees, 60 degrees and 120 degrees to obtain 3 diameters (6 radii), and the instantaneous flame radius Ru was obtained by averaging the 6 radius values.

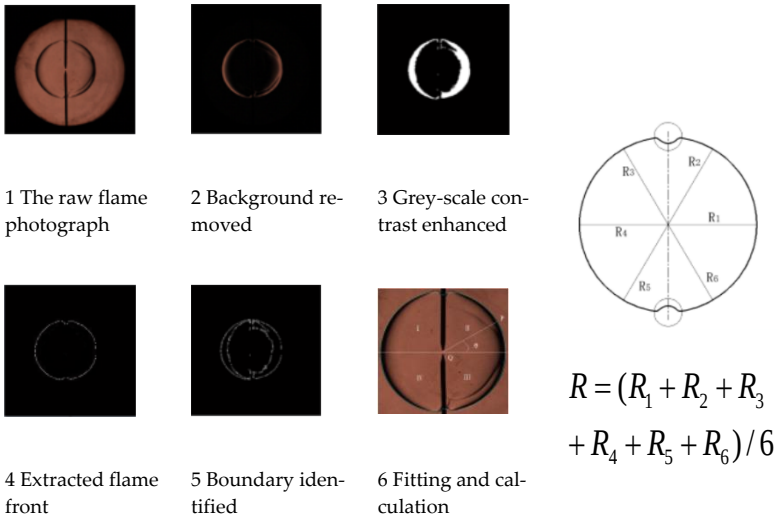

Figure 2. Diagram of flame radius extracting data calculating.

3.2. Data Calculation

In the spherical diffusion flame, the propagation rate of the tensile flame is given [22], shown below:

$$S_n = \mathrm{d}R_\mathrm{u}/\mathrm{d}t \tag{5}$$

where t is the time.

For the outwardly propagating spherical flame, the flame stretch rate can be simplified as follow [23]:

$$K = \mathrm{d}(\ln A)/\mathrm{d}t = 2S_\mathrm{n}/R_\mathrm{u} = \kappa S_\mathrm{n} \tag{6}$$

in which A is an infinitely small area on the flame and $\kappa = 2/\mathrm{Ru}$ is the curvature of the flame front.

To obtain the unstretched flame propagation velocity and the Markstein length, according to the literature [24], use the classical formula, shown as follow:

$$S_\mathrm{l} - S_\mathrm{n} = L_\mathrm{b}K \tag{7}$$

However, there is a certain theoretical error in this method, so the recommendation of Chen [25] is adopted. For most cases of the mixture with Lewis number $Le < 1$ or close to 1, the nonlinear method proposed by Kelley et al. [26] is as follows:

$$\ln(S_n) = \ln(S_l) - S_l L_b \kappa / S_n \tag{8}$$

For most cases of the mixture with $Le > 1$, another nonlinear formula [27] is used, shown as follow:

$$S_n = S_l - S_l L_b \kappa \tag{9}$$

where Le is as follows:

$$Le = \lambda / \rho_u c_p D_m = D_T / D_m \tag{10}$$

The un-stretched u_L can be calculated as follow [28]:

$$u_L = S_l(\rho_b / \rho_u) = S_l / \sigma \tag{11}$$

To further evaluate the influence of the coupling relationship of Pu, Tu and DR on u_L, this paper introduces the variation of laminar burning velocity Δu_{s1-s2}, defined as follow:

$$\Delta u_{s1-s2} = u_{s1} - u_{s2} \tag{12}$$

where u_{s1} and u_{s2} are the u_L of $s1$ and $s2$, respectively, and Δu_{s1-s2} is the variation of u_L between u_{s1} and u_{s2}.

To evaluate the changes in Tu, Pu and DR under the equivalent Δu_{s1-s2}, define equations as follow:

$$\Delta T_{s1-s2} = |T_{s1} - T_{s2}| \tag{13}$$

$$\Delta P_{s1-s2} = |P_{s1} - P_{s2}| \tag{14}$$

$$\Delta DR_{s1-s2} = |DR_{s1} - DR_{s2}| \tag{15}$$

where T_{s1}, T_{s2}, P_{s1}, P_{s2}, DR_{s1} and DR_{s2} represent the initial temperatures, initial pressures and dilution rates for the u_L of $s1$ and $s2$, respectively, and ΔT_{s1-s2}, ΔP_{s1-s2} and ΔDR_{s1-s2} are the corresponding Tu, Pu and DR of the variation in u_L between u_{s1} and u_{s2}.

To further analyse the influence of the coupling relationship of Pu, Tu and DR on the u_L, define the equations as follow:

$$RT_{s1-s2} = \frac{\Delta u_{s1-s2}}{\Delta T_{s1-s2}} \tag{16}$$

$$RP_{s1-s2} = \frac{\Delta u_{s1-s2}}{\Delta P_{s1-s2}} \tag{17}$$

$$RDR_{s1-s2} = \frac{\Delta u_{s1-s2}}{\Delta DR_{s1-s2}} \tag{18}$$

where, RT_{s1-s2}, RP_{s1-s2} and RDR_{s1-s2} represent the variations in u_L between u_{s1} and u_{s2} per unit temperature, unit pressure and unit dilution rate, respectively.

3.3. Chemical Kinetic Model

Chemkin (GRI_mech 3.0) was applied in this study. GRI_mech is a series of mechanisms aiming at combustion of methane that were proposed by Gas Research Institute, and GRI_mech 3.0 is the latest version. GRI_mech 3.0 mechanism contains 53 components and 325 elementary reactions and works well in the combustion of methane, carbon monoxide, hydrogen, etc.

4. Results and Discussion

Analysis of Laminar Burning Velocities Distribution of Natural Gas

Figure 3a shows the data comparison between the test and simulation. The results exhibit very good consistency between the simulated and measured values of u_L. It can be seen from the figure that the maximum error between the simulation model and the test results is 5%, within a reliable range [29–31]. To further improve the accuracy of the simulated values, Figure 3b shows the deviation of u_L measured by different groups from that predicted by the simulation based on GRI_mech 3.0. The results show that the difference in u_L between the simulated data (0.3 MPa and 323 K) and HASSAN's [32] and Halter's [9] (0.3 MPa and 298 K) is found to be within 4.7 cm/s at a temperature difference of 25 K. Good agreement is found between our data and Cai's [33] measurements except for the Φ of 0.7, where our u_L is 2.9 cm/s (error 9%) higher, as the temperature difference is 5 K. The deviation in numerical data is only slightly larger than that of Hinton's [34], especially when the equivalent is relatively high, but the maximum difference is only 5 cm/s. It can be seen that the simulation model maintains good consistency with the experimental results and literature data and can be used for analysis under certain working conditions.

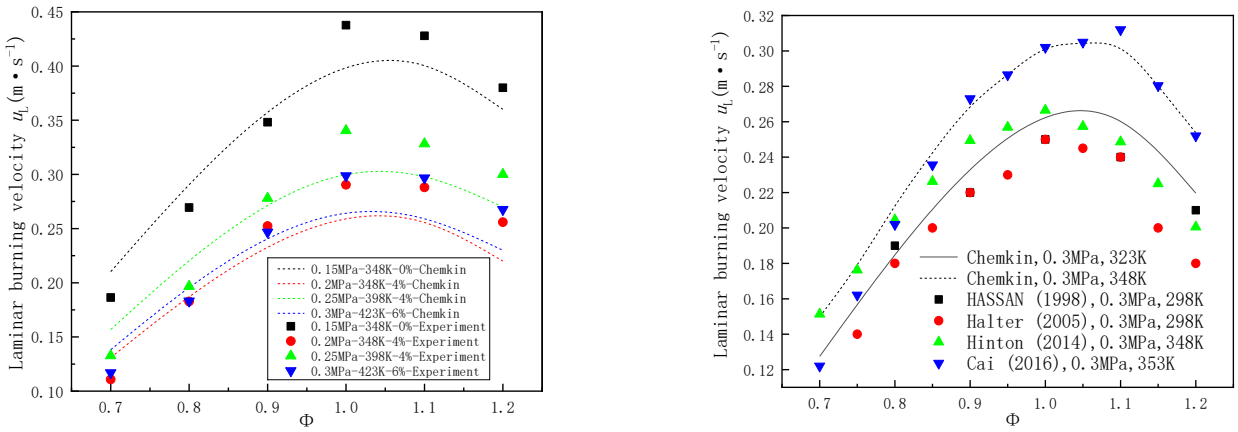

Figure 3. Validation of present simulation studies: (**a**) compared with experimental data and (**b**) compared with previous data.

Figure 4 shows the equivalent distribution pattern of u_L under the coupling effect of Tu and Pu when the equivalence ratios are 0.9, 1.0, 1.1 and 1.2 and when DR is 0%. As shown in the figure in the temperature range of 323–423 K, the pressure range of 0.1–0.3 MPa and Φ of 0.9–1.2, the ranges of u_L are 23.5–59.6 cm/s, 26.6–65.4 cm/s, 26.8–65.8 cm/s and 21.9–59.6 cm/s. With the increase in Φ, the variations in u_L are 36.1 cm/s, 38.8 cm/s, 39 cm/s and 37.7 cm/s, respectively, showing a trend increasing first and then decreasing. The maximum value occurs around Φ of 1.1. In addition, from the high-temperature and low-pressure area to the low-temperature and high-pressure area, u_L shows a clear downward trend, and as the temperature increases, the pressure decreases and u_L changes faster, that is, a larger rate of change in u_L in the high-temperature and low-pressure area.

The feature points in the u_L range of 32.53–46.06 cm/s were further extracted to analyse the variation pattern of the u_L corresponding to Φ. As illustrated in Figure 5, under a certain variation value of u_L, the corresponding Pu tends to increase first and then decrease, and the corresponding Tu decreases first and then increases as Φ increases. The trend shows that, with the increase in Φ, the isoline of u_L moves to the high-pressure and low-temperature region first and then moves to the low-pressure and high-temperature region around Φ of 1.1. Figure 6 shows the rate of change R in u_L in the velocity range of 32.53–46.06 cm/s. It can be seen from the figure that $R_{46.6–41.55} > R_{41.55–37.04} > R_{37.04–32.53}$, which indicates that, in the range of Φ at 0.9–1.2, the greater the u_L, the greater the rate of change R for u_L.

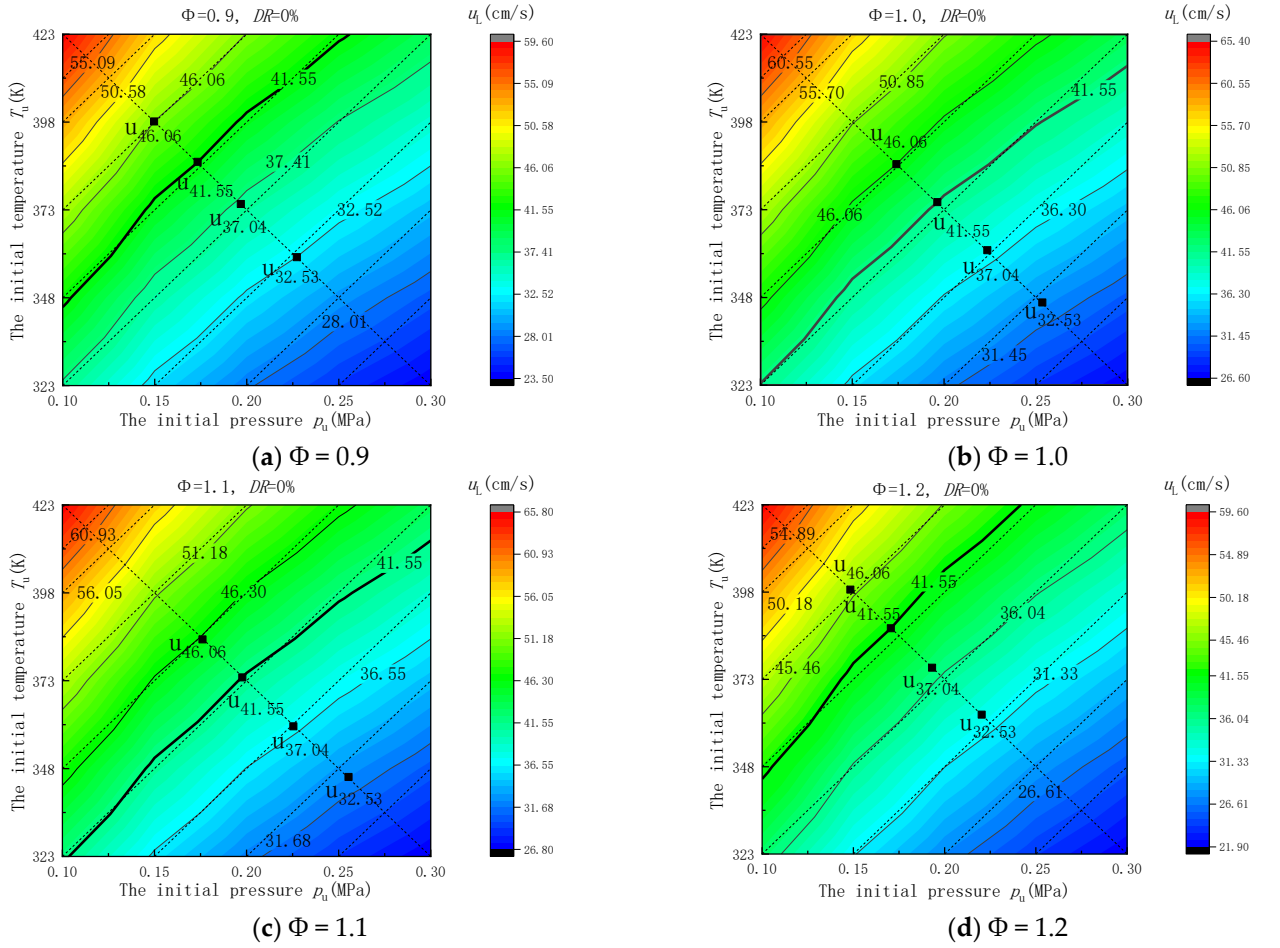

Figure 4. Equivalent distribution pattern of u_L under the coupling effect of Tu and Pu when the equivalence ratios are 0.9, 1.0, 1.1 and 1.2 and when dilution rate (DR) is 0%.

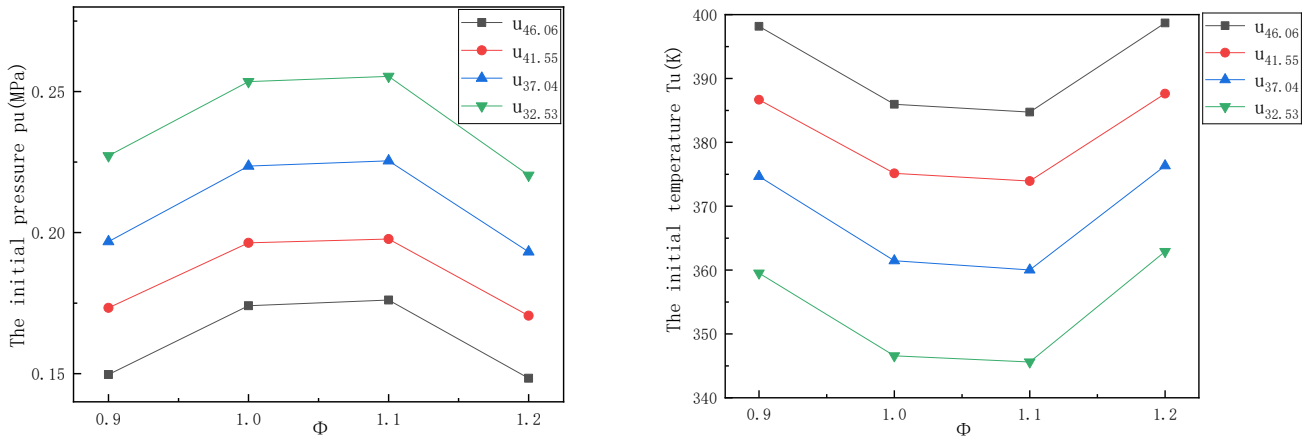

Figure 5. Equivalent variation of u_L corresponding to the initial condition change with Φ.

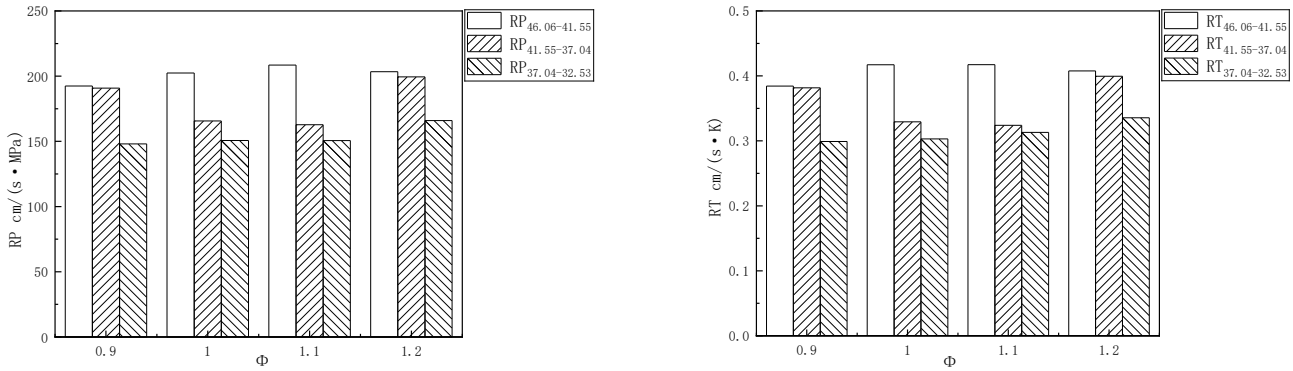

Figure 6. The rate of change R of u_L corresponding to Φ.

The auxiliary dashed curves in Figure 4 stand for the equivalent effect on the u_L of Tu and Pu. The specific equivalent relationship is that the Tu change of ΔT = 25 K and the Pu change of ΔP = 0.05 MPa have equivalent effects on the same variation value of u_L. The intersection of the isolines of u_L and the auxiliary dashed curves in the figure indicates that Tu and Pu have an equal influence weight on u_L at this point. All the equal weight intersection points in the figure are extracted and fitted into curves (refer to Figure 7); three regions are formed by equal weight curves. Among them, region II is the area where Pu has a greater influence on u_L, and region I and region III are the areas where Tu has a greater influence on u_L. As Φ increases, the equal weight curves of Tu and Pu exhibit different movement patterns. Refer to the figure, as Φ increases and Tu is less than 384 K, the low-pressure equal weight curve (Pu = 0.12–0.15 MPa) gradually moves toward a higher Pu but the increase rate changes more slowly with the increase in Tu. When Tu is greater than 384 K and Φ is 1.1, Pu of the low-pressure equal weight curve reaches the maximum. As such, with the Φ increases, the area of region I below a Tu of 384 K gradually increases, that is, the area in which the initial temperature influence weight is greater gradually increases. In the initial temperature above 384 K of region I, as Φ increases, the area of the region with the greater initial temperature influence weight increases first and then decreases. Furthermore, as Φ increases and the initial temperature is greater than 412 K, the high-pressure equal weight curve (Pu = 0.19–0.22 MPa) gradually moves toward a higher Pu. When the initial temperature is in the range of 342–412 K and Φ is 1.1, the Pu of the high-pressure equal weight curve reaches the minimum. When the initial temperature is lower than 342 K and Φ is 1.2, the Pu of the high-pressure equal weight curve reaches the minimum. Therefore, as Φ increases, the area in which the initial temperature is larger than 412 K with a greater initial temperature influence weight gradually decreases. While the initial temperature is below 384 K, the area with the greater initial temperature influence weight increases.

Figure 8 shows the equivalent distribution pattern of u_L under the coupling effect of initial temperature and Pu when Φ is 1.0 and when DR is 0–16%. Under the temperature range of 323–423 K; the pressure range of 0.1–0.3 MPa; and the dilution rates of 0, 4%, 8%, 12%, 14% and 16%, the ranges of u_L are 26.6–65.4 cm/s, 19.1–49.4 cm/s, 13.5–37.2 cm/s, 9.35–27.7 cm/s, 7.7–23.75 cm/s and 6.25–20.3 cm/s. As DR increases, the variations in u_L are 38.8 cm/s, 30.3 cm/s, 23.7 cm/s, 18.35 cm/s, 16.05 cm/s and 14.05 cm/s, showing a gradually decreasing trend. It can be seen from the figure that u_L in the high-temperature and low-pressure region is still greater than that in the low-temperature and high-pressure region and that the increase in DR only affects the rate of change in u_L. That is, although the higher the u_L, the greater the rate of change in u_L, but the increase in DR will weaken the increase in the rate of change in u_L.

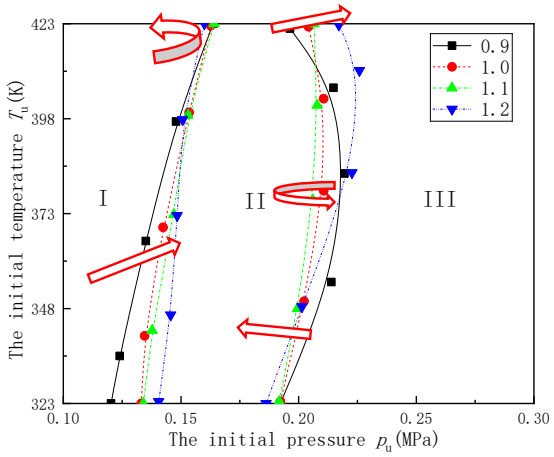

Figure 7. Variation pattern of the equal weight curve corresponding to Φ with ΔT = 25 K and ΔP = 0.05 MPa.

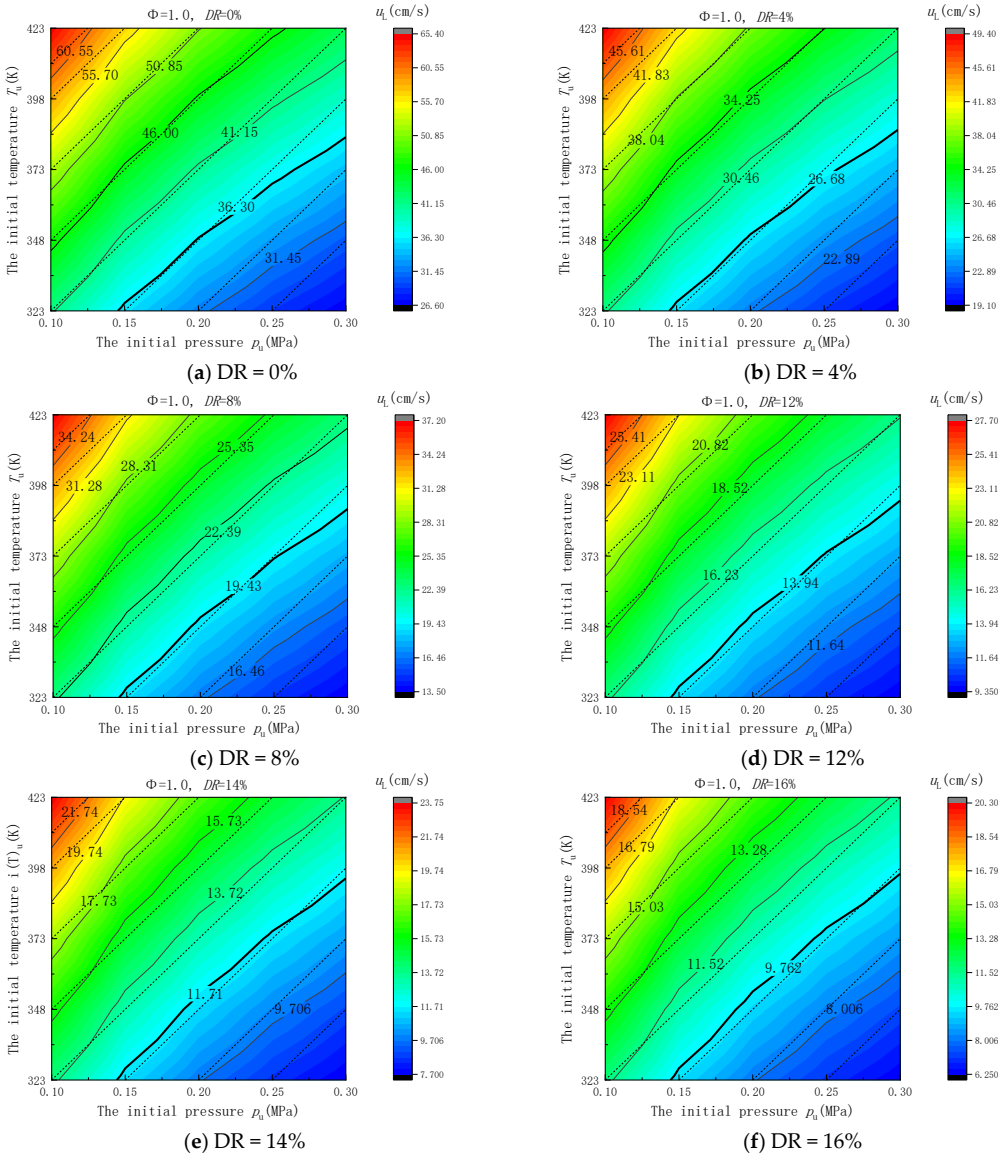

(**a**) DR = 0% (**b**) DR = 4%

(**c**) DR = 8% (**d**) DR = 12%

(**e**) DR = 14% (**f**) DR = 16%

Figure 8. The equivalent distribution pattern of u_L under the coupling effect of Tu and Pu when Φ is 1.0 and when the dilution rates are 0%, 4%, 8%, 12%, 14% and 16%.

Figure 9 shows the equal weight curve changes with the DR under the coupling effect of initial temperature and Pu. As illustrated, with the increase in DR when the initial temperature is greater than 350 K, the low-pressure equal weight curve (Pu = 0.125–0.165 MPa) gradually moves toward the lower Pu area and, as Tu increases, the increase rate slowly grows. When the initial temperature is lower than 350 K and DR is 14%, Pu of the low-pressure equal weight curve reaches the minimum. It can be seen that, as the DR increases, the area of region I above the initial temperature of 350 K gradually decreases, that is, the area with a greater initial temperature influence weight gradually decreases. Additionally, with the increase in DR, the high-pressure equal weight curve (Pu = 0.18–0.3 MPa) gradually moves toward the higher Pu area and, as Tu increases, the increase rate changes more slowly with the increase in initial temperature. As such, with the increase in DR, the area with the greater initial temperature influence weight gradually decreases and the decrease rate gradually decreases.

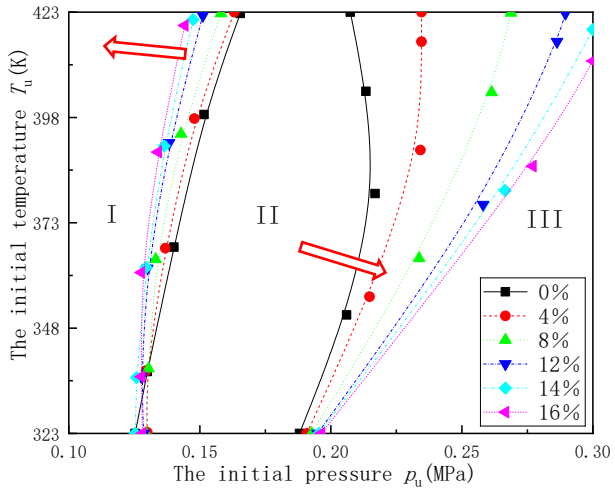

Figure 9. Variation pattern of the equal weight curve corresponding to DR with ΔT = 25 K and ΔP = 0.05 MPa.

Figure 10 shows the equivalent distribution pattern of u_L under the coupling effect of Tu and DR when Φ is 1.0 and when Pu is 0.1–0.25 MPa. The figure indicates that u_L gradually decreases from the high-temperature and low-dilution rate area to the low-temperature and high-dilution rate area. When Pu are 0.1 MPa, 0.15 MPa, 0.2 MPa and 0.25 MPa, the ranges of u_L are 22.6–65.4 cm/s, 19.0–56.9 cm/s, 16.6–51.1 cm/s and 14.9–46.7 cm/s. With the increase in Pu, the variations in u_L are 42.8 cm/s, 37.9 cm/s, 34.5 cm/s and 31.8 cm/s, respectively, exhibiting a gradually decreasing trend. The larger the Pu, the smaller the variation in u_L as well as the rate of change in u_L. In addition, the figure shows fine parallelism of the isolines of u_L, indicating that the coupling effect of DR and Tu exhibits a relatively stable isometric relationship and hardly changes with the variation in Pu. The measurements show that, when DR increases (or decreases) by 2% and the initial temperature increases (or decreases) by 29 K, an equal u_L can be obtained.

The feature points in the u_L range of 29.54–40.82 cm/s were further extracted to analyse the variation pattern of u_L corresponding to Pu. As shown in Figure 11, when the variation in u_L is constant, the corresponding DR decreases with the increase in Pu and the initial temperature increases with the increase in Pu. This clearly shows that, with the increase in Pu, the isoline of u_L moves to the low-dilution rate and high-temperature area. Figure 12 shows the rate of change R of u_L in the velocity range of 29.54–40.82 cm/s. It can be seen from the figure that $R_{40.82\text{-}37.06} > R_{37.06\text{-}33.30} > R_{33.30\text{-}29.54}$, which indicates that, in the range of Φ 0.1–0.25, the greater the u_L, the greater the rate of change R in u_L.

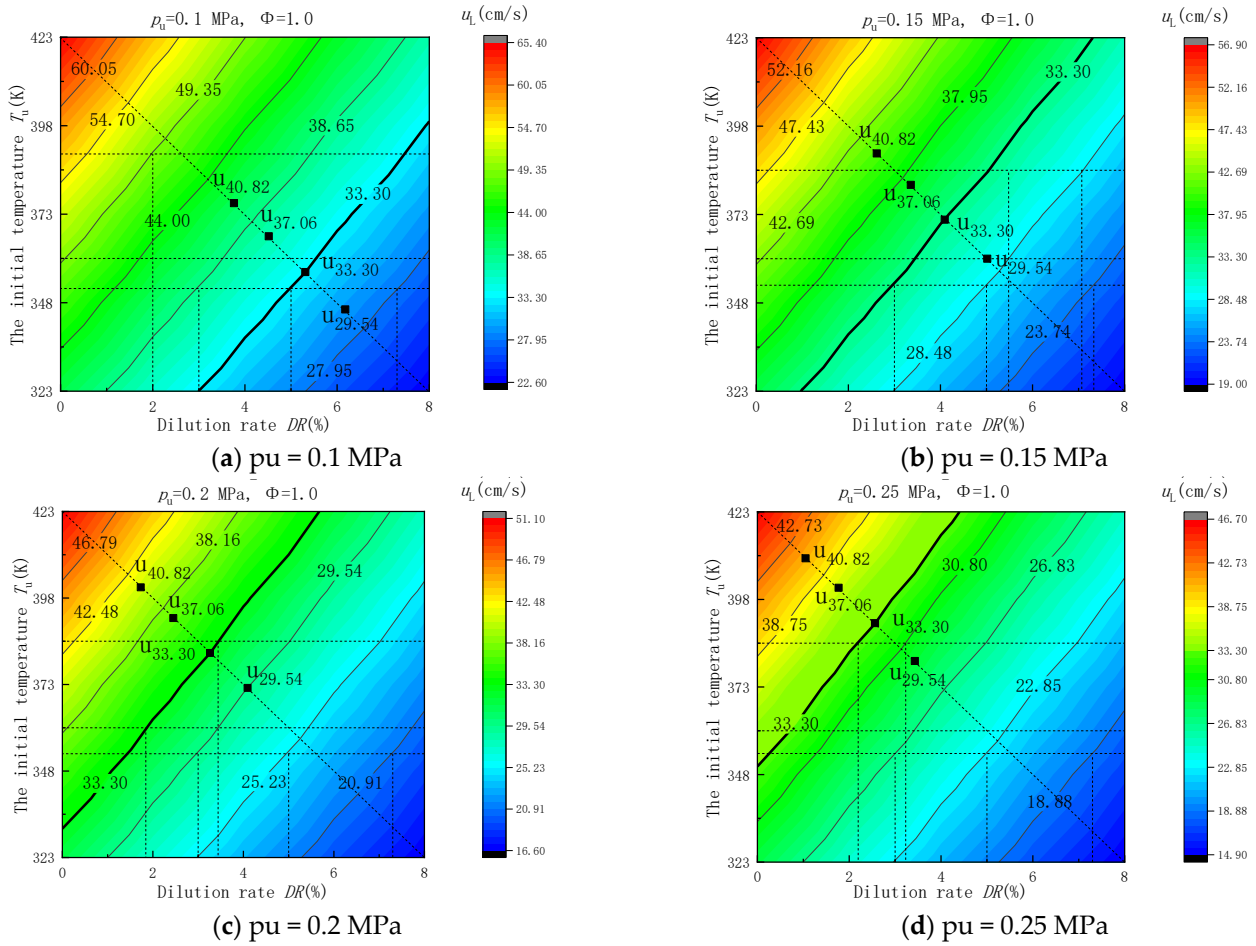

Figure 10. Equivalent distribution pattern of u_L under the coupling effect of Tu and DR when Φ is 1.0 and when the initial pressures are 0.1 MPa, 0.15 MPa, 0.2 MPa and 0.25 MPa.

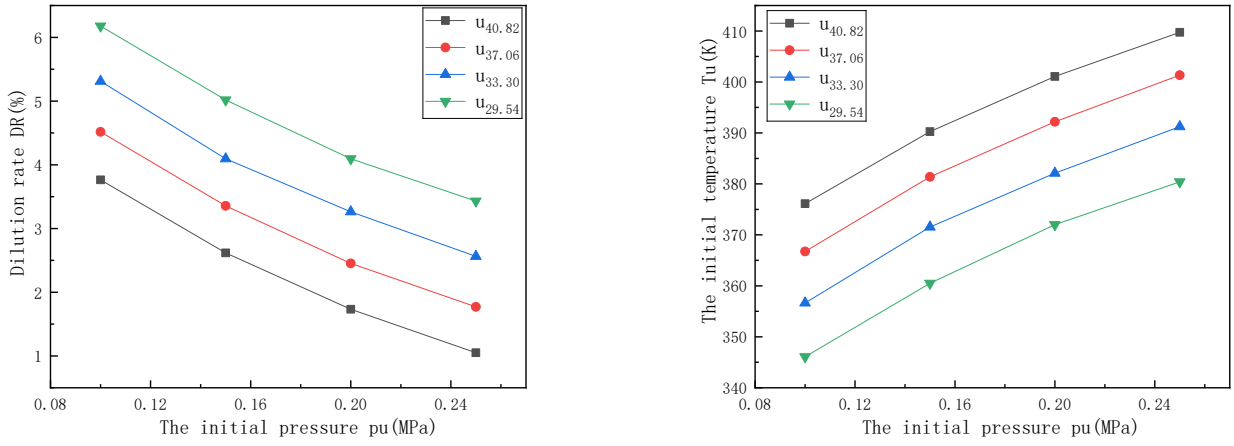

Figure 11. Equivalent variation of u_L corresponding to the initial condition change with Pu.

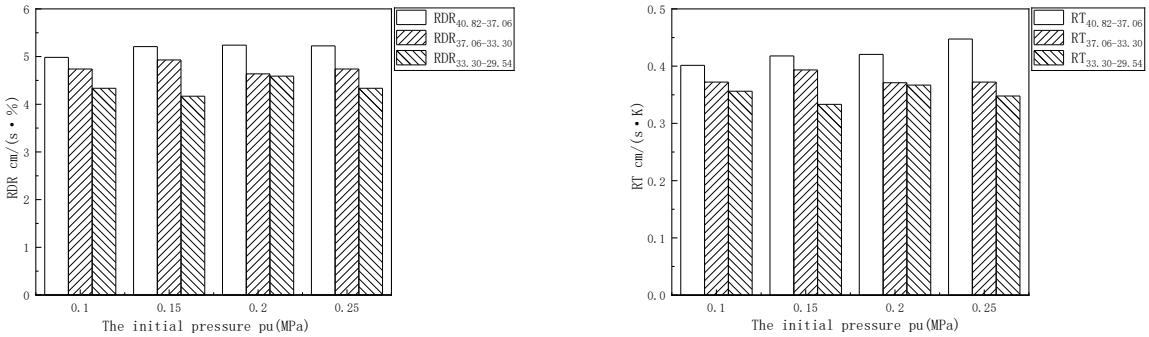

Figure 12. The rate of change R of the u_L corresponding to the Pu.

Figure 13 shows the equivalent distribution pattern of u_L under the coupling effect of Tu and DR when Φ is 1.0 and when the range of the initial temperature is 348–423 K. The figure indicates that u_L gradually decreases from the low-pressure and low-dilution rate area to the high-pressure and high-dilution rate area. When the initial temperatures are 348 K, 373 K, 398 K and 423 K, the ranges of u_L are 15.50–46.80 cm/s, 17.80–52.60 cm/s, 20.2–58.8 cm/s and 22.8–65.4 cm/s. With the increase in initial temperature, the variations in u_L are 31.3 cm/s, 34.8 cm/s, 38.6 cm/s and 42.6 cm/s, respectively, exhibiting a gradually increasing trend. The larger the initial temperature, the greater the variation in u_L as well as the rate of change R in u_L. In addition, from the high-pressure and high-dilution rate area to the low-pressure and low-dilution rate area, u_L shows a clear upward trend, and as Pu and DR decrease, u_L changes faster, that is, a larger rate of change in u_L in the low-pressure and low-dilution rate area.

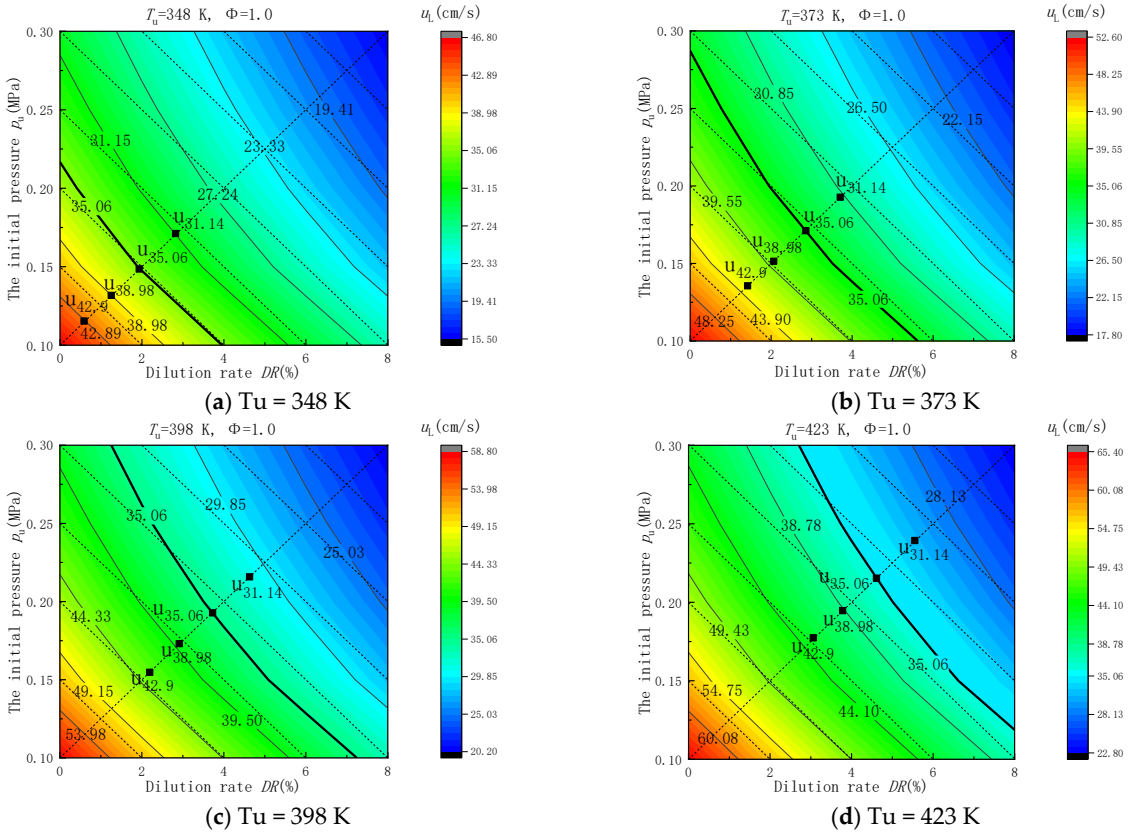

Figure 13. Equivalent distribution pattern of u_L under the coupling effect of Pu and DR when Φ is 1.0 and when the initial temperatures are 348 K, 373 K, 398 K and 423 K.

The feature points in the u_L range of 31.14–42.9 cm/s were further extracted to analyse the variation pattern of u_L corresponding to Pu. As shown in Figure 14, when the variation in u_L is constant, the corresponding DR and Pu decrease with the increase in the initial temperature. This clearly shows that, with the increase in initial temperature, the isoline of u_L moves to the high-pressure and high-dilution rate area. Figure 15 shows the rate of change R in u_L in the velocity range of 31.14–42.9 cm/s. It can be seen from the figure that $R_{42.90\text{-}38.98} > R_{38.98\text{-}35.06} > R_{35.06\text{-}31.14}$, which indicates that, in the range of initial temperatures 348–423 K, the greater the u_L, the greater the rate of change R in u_L.

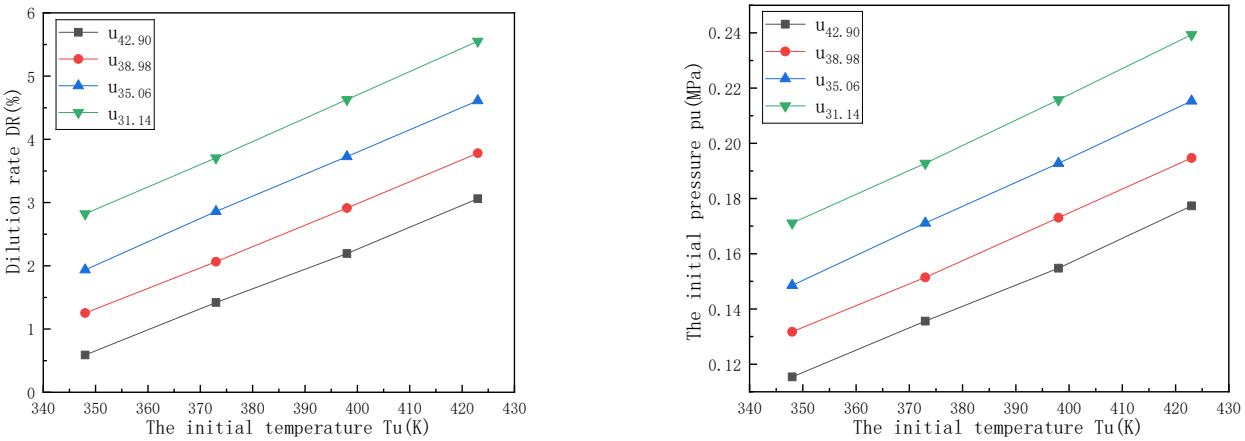

Figure 14. Equivalent variation in u_L corresponding to the initial condition change with Tu.

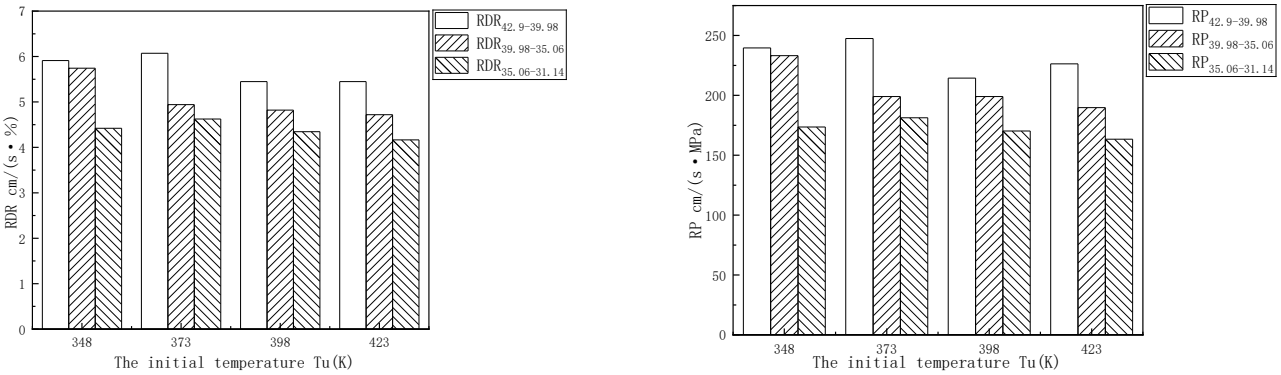

Figure 15. The rate of change R in u_L corresponding to Tu.

The auxiliary dashed curves in Figure 13 stand for the equivalent effect on the u_L of Pu and DR. The specific equivalent relationship is that the Pu change of $\Delta P = 0.05$ MPa and the DR change of 2% have equivalent effects on the same variation value of u_L. The intersection of the isolines of u_L and the auxiliary dashed curves in the figure indicates that Pu and DR have an equal influence weight on u_L at this point. All the equal weight intersection points in the figure are extracted and fitted onto curves (refer to Figure 16), and two regions are formed by equal weight curves. Region I is the area where the DR has a greater influence on u_L, while in region II, Pu has a greater influence on u_L. This shows that, under the influence of the coupling effect of Pu and DR on u_L, Pu of the low-pressure and high-dilution rate area has a greater weight on u_L. As the initial temperature increases, the equal weight curves of Pu and DR exhibit different movement patterns.

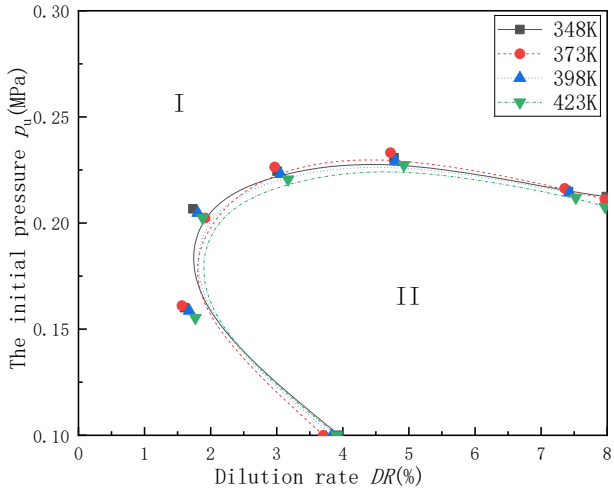

Figure 16. Variation pattern of the equal weight curve corresponding to Tu with ΔDR = 2% and ΔP = 0.05 MPa.

5. Conclusions

Due to the initial temperature having a promoting effect on laminar burning velocity while the initial pressure and dilution rate have an inhibitory effect on laminar burning velocity, equal laminar burning velocities can be obtained by initial condition coupling with different temperatures, pressures and dilution rates. This paper analysed the equivalent distribution pattern of the laminar burning velocity and the variation pattern of the equal weight curve by coupling effect of the initial pressure (0.1–0.3 MPa), initial temperature (323–423 K) and dilution rate (0–16%). The main conclusions are summarized as follows:

1. As the initial temperature increases and the initial pressure decreases, the rate of change in laminar burning velocity increases. Moreover, the increase in equivalent ratio makes the variation of laminar burning velocity show a trend increasing first and then decreasing and the maximum value is reached when Φ = 1.1, while with the increase in the dilution rate, the variation in laminar burning velocity gradually decreases and the isoline of laminar burning velocity gradually moves towards the high-temperature and low-pressure area.
2. The equivalent effect of initial condition coupling can obtain equal laminar burning velocity with the dilution rate increasing (or decreasing) by 2% and the initial temperature increasing (or decreasing) by 29 K. Additionally, the variation in laminar burning velocity tends to decrease with the increase in initial pressure, and the isoline of laminar burning velocity gradually moves towards the high-temperature and low-dilution rate area.
3. With the dilution rate and the initial pressure decreasing, the rate of change in laminar burning velocity increases. Additionally, the variation in laminar burning velocity tends to increase with the increase in initial temperature, and the isoline of laminar burning velocity gradually moves towards the high-pressure and high-dilution rate area.
4. As the equivalence ratio increases when the initial temperature is less than 384 K, the area with the greater initial temperature influence weight gradually increases, and when it exceeds 384 K, the area increases first and then decreases; when the initial temperature is greater than 412 K, the area gradually decreases with the increase in equivalence ratio, while when the initial temperature is less than 342 K, the area gradually increases with the increase in equivalence ratio.
5. With the increase in dilution rate, the area with the greater initial temperature influence weight gradually decreases and the decrease rate gradually decreases. In the low-pressure and high-dilution rate region, the initial pressure has a greater influence weight on laminar burning velocity, while in the high-pressure and low-dilution rate region, the dilution rate has a greater influence weight on laminar burning velocity.

Author Contributions: Conceptualization, X.W., P.W. and Z.H.; methodology, X.W., Z.Z. and W.Y.; software, P.W. and Y.Q.; validation, W.Y., Z.H. and P.W.; formal analysis, X.W. and P.W.; investigation, Z.Z.; resources, Z.Z.; data curation, Y.Q.; writing—original draft preparation, P.W.; writing—review and editing, X.W., W.Y. and Z.H.; visualization, P.W.; supervision, W.Y.; project administration, X.W.; funding acquisition, W.Y. and Z.H. All authors have read and agreed to the published version of the manuscript.

Funding: This work was supported by the National Natural Science Foundation of China under grant No. 51776177. The authors would like to express sincere appreciation to Wei Tian, Zinong Zuo, Kun Liang, Bang Xiao and Dongjian Zeng for their assistance.

Institutional Review Board Statement: Not applicable.

Informed Consent Statement: Informed consent was obtained from all subjects involved in the study.

Data Availability Statement: Data is contained within the article.

Conflicts of Interest: The authors declare no conflict of interest.

Abbreviations

Pu	Initial pressure, MPa
Tu	Initial temperature, K
u_L	Laminar burning velocity, $m \cdot s^{-1}$
DR	Dilution rate
Φ	Equivalence ratio
CVC	Constant volume chamber
EGR	Exhaust gas recirculation
R_u	Instantaneous flame radius: mm
S_n	Stretched flame propagation speed, $m \cdot s^{-1}$
κ	Curvature of spherical flame, mm^{-1}
K	Stretch rate, s^{-1}
L_b	Markstein length, mm
S_l	Unstretched flame propagation speed, $m \cdot s^{-1}$
Le	Lewis number
λ	Thermal conductivity, $W \cdot (m \cdot K)^{-1}$
ρu	Density of unburned gas, $kg \cdot m^{-3}$
c_p	Specific heat capacity, $J \cdot (kg \cdot K)^{-1}$
D_m	Mass diffusion coefficient, $m^2 \cdot s^{-1}$
D_T	Thermal diffusion coefficient, $m^2 \cdot s^{-1}$
ρb	Density of burned gas, $kg \cdot m^{-3}$
σ	Thermal expansion ratio

References

1. Verma, G.; Prasad, R.K.; Agarwal, R.A.; Jain, S.; Agarwal, A.K. Experimental investigations of combustion, performance and emission characteristics of a hydrogen enriched natural gas fuelled prototype spark ignition engine. *Fuel* **2016**, *178*, 209–217. [CrossRef]
2. Zheng, J.; Wang, J.; Zhao, Z.; Wang, D.; Huang, Z. Effect of equivalence ratio on combustion and emissions of a dual-fuel natural gas engine ignited with diesel. *Appl. Therm. Eng.* **2019**, *146*, 738–751. [CrossRef]
3. Moon, S. Potential of direct-injection for the improvement of homogeneous-charge combustion in spark-ignition natural gas engines. *Appl. Therm. Eng.* **2018**, *136*, 41–48. [CrossRef]
4. Wang, S.; Wang, Z.; He, Y.; Han, X.; Sun, Z.; Zhu, Y.; Costa, M. Laminar burning velocities of CH4/O-2/N-2 and oxygen-enriched CH4/O-2/CO2 flames at elevated pressures measured using the heat flux method. *Fuel* **2020**, *259*, 116152. [CrossRef]
5. Hu, E.; Xu, Z.; Gao, Z.; Xu, J.; Huang, Z. Experimental and numerical study on laminar burning velocity of gasoline and gasoline surrogates. *Fuel* **2019**, *256*. [CrossRef]
6. Van Treek, L.; Lavadera, M.L.; Seidel, L.; Mauss, F.; Konnov, A.A. Experimental and modelling study of laminar burning velocity of aqueous ethanol. *Fuel* **2019**, *257*, 116069. [CrossRef]
7. Han, Z.; Zhu, Z.; Wang, P.; Liang, K.; Zuo, Z.; Zeng, D. The Effect of Initial Conditions on the Laminar Burning Characteristics of Natural Gas Diluted by CO2. *Energies* **2019**, *12*, 2892. [CrossRef]
8. Hermanns, R.R.; Konnov, A.A.; Bastiaans, R.R.; De Goey, L.P.; Lucka, K.; Kohne, H. Effects of temperature and composition on the laminar burning velocity of CH4+H2+O2+N2 flames. *Fuel* **2010**, *89*, 114–121. [CrossRef]
9. Halter, F.; Chauveau, C.; Djeballi-Chaumeix, N.; Gokalp, I. Characterization of the effects of pressure and hydrogen concentration on laminar burning velocities of methane-hydrogen-air mixtures. *Proc. Combust. Inst.* **2005**, *30*, 201–208. [CrossRef]

10. Xie, M.; Fu, J.; Zhang, Y.; Shu, J.; Shu, J.; Liu, J.; Zeng, D. Numerical analysis on the effects of CO2 dilution on the laminar burning velocity of premixed methane/air flame with elevated initial temperature and pressure. *Fuel* **2020**, *264*, 116858. [CrossRef]
11. Chan, Y.L.; Zhu, M.M.; Zhang, Z.Z.; Liu, P.F.; Zhang, D.K. The Effect of CO2 Dilution on the Laminar Burning Velocity of Premixed Methane/Air Flames. *Energy Procedia* **2015**, *75*, 3048–3053. [CrossRef]
12. Zhou, Q.; Cheung, C.S.; Leung, C.W.; Li, X.; Huang, Z. Effects of diluents on laminar burning characteristics of bio-syngas at elevated pressure. *Fuel* **2019**, *248*, 8–15. [CrossRef]
13. Huang, Z.; Zhang, Y.; Zeng, K.; Liu, B.; Wang, Q.; Jiang, D. Measurements of laminar burning velocities for natural gas-hydrogen-air mixtures. *Combust. Flame* **2006**, *146*, 302–311. [CrossRef]
14. Dirrenberger, P.; Le Gall, H.; Bounaceur, R.; Herbinet, O.; Glaude, P.A.; Konnov, A.; Battin-Leclerc, F. Measurements of Laminar Flame Velocity for Components of Natural Gas. *Energy Fuels* **2011**, *25*, 3875–3984. [CrossRef]
15. Li, H.-M.; Li, G.-X.; Sun, Z.-Y.; Zhai, Y.; Zhou, Z.-H. Measurement of the laminar burning velocities and markstein lengths of lean and stoichiometric syngas premixed flames under various hydrogen fractions. *Int. J. Hydrog. Energy* **2014**, *39*, 17371–17380. [CrossRef]
16. Qian, Y. *Research on the Influence of Key Parameters on the Equivalent Effect of Natural Gas-CO2-Air Premixed Combustion*; Xi hua University: Chengdu, China, 2018.
17. Zhang, X.; Huang, Z.; Zhang, Z.; Zheng, J.; Yu, W.; Jiang, D. Measurements of laminar burning velocities and flame stability analysis for dissociated methanol-air-diluent mixtures at elevated temperatures and pressures. *Int. J. Hydrog. Energy* **2009**, *34*, 4862–4875. [CrossRef]
18. Wang, J.; Huang, Z.; Kobayashi, H.; Ogami, Y. Laminar burning velocities and flame characteristics of CO-H-2-CO2-O-2 mixtures. *Int. J. Hydrog. Energy* **2012**, *37*, 19158–19167. [CrossRef]
19. Vu, T.M.; Park, J.; Kwon, O.B.; Bae, D.S.; Yun, J.H.; Keel, S.I. Effects of diluents on cellular instabilities in outwardly propagating spherical syngas-air premixed flames. *Int. J. Hydrogen Energy* **2010**, *35*, 3868–3880. [CrossRef]
20. Luo, Z.; Hao, Q.; Wang, T.; Li, R.; Cheng, F.; Deng, J. Experimental study on the deflagration characteristics of methane-ethane mixtures in a closed duct. *Fuel* **2020**, *259*, 116295. [CrossRef]
21. Lu, L.; Pei, Y.; Qin, J.; Zuo, Z.; Xu, H. Laminar burning characteristics of premixed methane-dissociated methanol-diluent mixtures. *Int. J. Hydrogen Energy* **2019**, *44*, 11097–11110. [CrossRef]
22. Zuo, Z.; Pei, Y.; Qin, J.; Lu, L.; Xu, H. Impact of dissociated Methanol addition on premixed Toluene reference fuel-air mixtures in a constant-volume chamber. *Int. J. Hydrogen Energy* **2018**, *43*, 6745–6755. [CrossRef]
23. Law, C.K.; Sung, C.J. Structure, aerodynamics, and geometry of premixed flamelets. *Prog. Energy Combust. Sci.* **2000**, *26*, 459–505. [CrossRef]
24. Liao, S.Y.; Jiang, D.M.; Huang, Z.H.; Zeng, K.; Cheng, Q. Determination of the laminar burning velocities for mixtures of ethanol and air at elevated temperatures. *Appl. Therm. Eng.* **2007**, *27*, 374–380. [CrossRef]
25. Chen, Z. On the extraction of laminar flame speed and Markstein length from outwardly propagating spherical flames. *Combust. Flame* **2011**, *158*, 291–300. [CrossRef]
26. Kelley, A.P.; Law, C.K. Nonlinear effects in the extraction of laminar flame speeds from expanding spherical flames. *Combust. Flame* **2009**, *156*, 1844–1851. [CrossRef]
27. Markstein, H.G. Experimental and theoretical studies of flame-front stability. *Dyn. Curved Front.* **1988**, *18*, 413–423. [CrossRef]
28. Bradley, D.; Lawes, M.; Liu, K.; Verhelst, S.; Woolley, R. Laminar burning velocities of lean hydrogen-air mixtures at pressures up to 1.0 MPa. *Combust. Flame* **2007**, *149*, 162–172. [CrossRef]
29. Han, X.; Wang, Z.; Wang, S.; Whiddon, R.; He, Y.; Lv, Y.; Konnov, A.A. Parametrization of the temperature dependence of laminar burning velocity for methane and ethane flames. *Fuel* **2019**, *239*, 1028–1037. [CrossRef]
30. Varghese, R.J.; Kolekar, H.; Kumar, S. Laminar burning velocities of H2/CO/CH4/CO2/N2 -air mixtures at elevated temperatures. *Int. J. Hydrogen Energy* **2019**, *44*, 12188–12199. [CrossRef]
31. Rau, F.; Hartl, S.; Hasse, C. Numerical and experimental investigation of the laminar burning velocity of biofuels at atmospheric and high-pressure conditions. *Fuel* **2019**, *247*, 250–256. [CrossRef]
32. Hassan, M.I.; Aung, K.T.; Kwon, O.C.; Faeth, G.M. Faeth, Properties of Laminar Premixed Hydrocarbon/Air Flames at Various Pressures. *J. Propuls. Power* **1998**, *14*, 479–488. [CrossRef]
33. Cai, X.; Wang, J.; Zhang, W.; Xie, Y.; Zhang, M.; Huang, Z. Effects of oxygen enrichment on laminar burning velocities and Markstein lengths of CH4/O2/N2 flames at elevated pressures. *Fuel* **2016**, *184*, 466–473. [CrossRef]
34. Hinton, N.; Stone, R. Laminar burning velocity measurements of methane and carbon dioxide mixtures (biogas) over wide ranging temperatures and pressures. *Fuel* **2014**, *116*, 743–750. [CrossRef]